Journal of Power Sources 233 (2013) 252–258

Contents lists available at SciVerse ScienceDirect

Journal of Power Sources

journal homepage: www.elsevier.com/locate/jpowsour

Au–Pd nanoparticles supported on carbon fiber cloth as the electrocatalyst for H_2O_2 electroreduction in acid medium

Fan Yang [a], Kui Cheng [a], Tianhao Wu [b], Ying Zhang [a], Jinling Yin [a], Guiling Wang [a], Dianxue Cao [a,*]

[a] Key Laboratory of Superlight Material and Surface Technology of Ministry of Education, College of Material Science and Chemical Engineering, Harbin Engineering University, Harbin 150001, China
[b] ChenGeng Class, Harbin Engineering University, Harbin 150001, China

HIGHLIGHTS

- Flower-like Au–Pd NPs are electrodeposited on CFC via potential pulse technique.
- Au–Pd NPs show higher catalytic activity for H_2O_2 reduction than pure Au or Pd.
- Au–Pd NPs/CFC electrodes with different composition stoichiometry are obtained.

ARTICLE INFO

Article history:
Received 28 October 2012
Received in revised form
21 January 2013
Accepted 22 January 2013
Available online 29 January 2013

Keywords:
Flower-like gold–palladium nanoparticles
Carbon fiber cloth
Hydrogen peroxide
Electroreduction
Acid medium

ABSTRACT

A novel synthesis of Au–Pd alloy nanoparticles supported on carbon fiber cloth (Au–Pd NPs/CFC) via a potential pulse technique is presented. Different composition stoichiometry of Au–Pd nanoparticles are deposited from the aqueous solutions of $HAuCl_4/PdCl_2$ mixtures in molar ratios of 5:1, 2:1, 1:1, 1:2 and 1:5. The electrode is characterized by scanning electron microscopy coupled to energy dispersive X-ray analysis (SEM–EDX), transmission electron microscopy (TEM) and X-ray diffractometer (XRD). H_2O_2 electroreduction in H_2SO_4 solution on Au–Pd nanoparticles is studied by linear sweep voltammetry and chronoamperometry. The catalytic performance on different composition stoichiometry of Au–Pd nanoparticles increases with the increase of Pd content. Additionally, the flower-like Au–Pd NPs/CFC electrode exhibits the excellent catalytic properties and good stability to H_2O_2 electroreduction in acid solution, and it outperforms pure Au or Pd catalyst supported on carbon fiber cloth.

1. Introduction

Pd is one of the most used noble metals having outstanding catalytic properties which is similar to Pt. Being a more economic and plentiful metal than Pt [1], Au has been also investigated for its electrocatalytic activity [2–7], yet is demonstrated to be relatively less reactive due to the weak chemisorption properties [1,8]. On the other hand, Au is more electronegative compared to Pd or Pt [9] which could modify the strength of the surface adsorption in Pd-based alloys after the incorporation of Au. Very recently, Au is demonstrated to have the role to significantly improve the stability of the Pt and Pd [10].

In order to obtain the cooperative catalytic properties of Au and Pd, a class of Au catalysts coated or alloyed with Pd has been introduced. For example, Au–Pd alloys and Au–Pd core–shell nanoparticles were synthesized and examined. In recent years, Au–Pd bimetallic nanoparticles are known to have extraordinary catalytic activities in a large number of reactions [1,11–25]. The oxidation of benzyl alcohol to benzaldehyde can be accelerated by 10–100 times through the use of Au_{core}–Pd_{shell} (Au_cPd_s) nanoparticles in place of Pd or Au nanoparticles, respectively [26]. It is known that the properties of alloys could be readily influenced by tuning the size, shape, and composition of nanoparticle catalysts. In order to meet the need of better control, a variety of approaches have been reported on their preparation of Au–Pd nanoparticles such as co-reduction [15,27,28] and seed-mediated growth [1,18,29,30]. Zhang et al. [15] synthesized a series of Au–Pd nanoparticles (NPs) using mixed *n*-dodecylamine/tetraoctylphosphonium bromide ligands. Xu and co-workers [30] prepared nanoflowers with a Au core and Pd petals by reduction of Pd ions by hydroquinone in the presence of gold nanoparticles and polyvinylpyrrolidone.

Herein, we present a study on the synthesis and characterization of Au–Pd alloy nanoparticles supported on carbon fiber cloth (Au–Pd NPs/CFC). Flower-shaped Au–Pd alloy nanoparticles

* Corresponding author. Tel./fax: +86 451 82589036.
E-mail address: caodianxue@hrbeu.edu.cn (D. Cao).

0378-7753/$ – see front matter © 2013 Elsevier B.V. All rights reserved.
http://dx.doi.org/10.1016/j.jpowsour.2013.01.144

were readily prepared by potential pulse electrodeposition. Compared to other methods to prepare carbon-supported Au–Pd nanoparticles, using electrodeposition to synthesize and tune the size, shape, and composition of nanoparticle catalysts is facile and efficient. More importantly, electrocatalyst directly contacting with the carbon substrate could avoid many shortcomings such as not fully contacting with the solution due to the existence of binder. Moreover, we in detail discuss the shape, composition and catalytic performance of Au–Pd alloy nanoparticles at different electrodeposition conditions. H_2O_2 as a green powerful, carbon-free energy carrier has been used as oxidant in a fuel cell engine [31–37]. The performance of H_2O_2 electroreduction greatly influences the performance of fuel cells. The obtained Au–Pd NPs/CFC electrode demonstrated high catalytic activity and good stability for H_2O_2 electroreduction in H_2SO_4 solution which may be a candidate for the application in fuel cells.

2. Experimental

2.1. Reagents

Palladium (II) chloride ($PdCl_2$), chloroauric acid tetrahydrate ($HAuCl_4 \cdot 4H_2O$) (>99.9%), sulfuric acid (H_2SO_4), perchloric acid ($HClO_4$) and hydrogen peroxide (H_2O_2) were obtained from Enterprise Group Chemicals Reagent Co. Ltd. China. Carbon fiber cloth (thickness: 0.3 mm) was purchased from Shanghai Hesen electric Co., Ltd. All chemicals are analytical grade and were used as-received without further purification. Ultrapure water (Millipore, 18 MΩ cm) was used throughout the study.

2.2. Preparation and characterization of the Au–Pd NPs/CFC electrode

To deposit Au–Pd NPs on the carbon fiber cloth, the substrate was first immersed into acetone to degrease oil. In a novel synthesis of Au–Pd NPs, a 25 mL aqueous solution consisting of 0.05 mol L^{-1} $HClO_4$, 0.25 mol L^{-1} H_2SO_4 and 3.0 mmol L^{-1} of $HAuCl_4/PdCl_2$ mixtures in molar ratios of 5:1, 2:1, 1:1, 1:2 and 1:5 was used as the deposition solution. The mixed solution was deaerated with nitrogen gas for about 15 min. The preparation experiment was performed by potential pulse electrodeposition which were carried out in a three-electrode electrochemical cell controlled by computerized potentiostat (Autolab PGSTAT302, Eco Chemie). The CFC (1.0 × 1.0 cm) served as the working electrode, which was placed between two pieces of platinum foil (1.0 × 1.0 cm) in parallel as the counter electrodes. A saturated Ag/AgCl (3 mol dm^{-3} KCl) electrode was used as the reference electrode, and all potentials in this work were referred to this reference electrode.

The morphology of nanoparticles is influenced by the oxidation potential (the upper potential), the reduction potential (the lower potential), frequency and deposition time. In order to examine the influence of the deposition potential for both Au and Pd deposited on carbon fiber cloth (CFC), we first chose 0 V as the reduction potential (the lower potential) to make both Au and Pd deposit on CFC, and varied the upper potential from 0.8 to 1.5 V, the deposition time was set at 20 min and the solution concentration was maintained in 25 mL solution containing 2.5 mmol L^{-1} $PdCl_2$, 0.5 mmol L^{-1} $HAuCl_4$, 0.05 mol L^{-1} $HClO_4$, 0.25 mol L^{-1} H_2SO_4. It was found that, at high oxidation potential (e.g. 1.5 V), a small amount of Au–Pd alloy nanoparticles with smooth surface were formed on the CFC, instead of the flower-like nanoparticles. When the upper potential was reduced, the corrugated surface of Au–Pd nanoparticles was observed, and then the flower-like Au–Pd nanoparticles was formed at 1.3 V. When further reduced the upper potential to 0.8 V, the size of nanoparticles was increased to higher than 300 nm which was not in favor of improving the utilization of noble metal. The effect of the reduction potential was also investigated in the range of 0 V–0.35 V by fixing the oxidation potential at 1.3 V. It was found that the Au–Pd alloy nanoparticles morphology changed dramatically with the change of reduction potential. Besides, shortening the deposition time decreased the amount and size of nanoparticles. On the basis of the above results, we determined 1.3 V as the oxidation potential, 0 V as the reduction potential, and the frequency of the potential pulse was 100 Hz, the deposition time was 20 min.

The electrode morphology was characterized by a scanning electron microscope (SEM, JEOL JSM-6480) equipped with an energy-dispersive X-ray (EDX) analyzer and a transmission electron microscope (TEM, FEI TeccaiG2S-Twin, Philips). The structure was analyzed using an X-ray diffractometer (Rigaku TTR III) with Cu K radiation (λ = 0.1514178 nm). The metal loading was measured using an inductive coupled plasma emission spectrometer (ICP, Xseries II, Thermo Scientific). Au and Pd in the 1.0 cm^2 electrode were first dissolved in aqua regia solution and then diluted to 100 mL solution for the ICP measurement.

2.3. Electrochemical measurements

H_2O_2 electroreduction were performed in a three-electrode electrochemical cell with the same configuration as that for electrodeposition with the exception that the two Pt foil counter electrodes were placed behind D-porosity glass frits. The electrolyte for H_2O_2 electroreduction was H_2O_2-containing H_2SO_4 solution. The reported current densities were calculated using the geometrical area of the electrode. All solutions were made with analytical grade chemical reagents and ultra-pure water (Milli-Q 18 MΩ cm). All measurements were performed at ambient temperature (22 ± 2 °C) under N_2 atmosphere.

3. Results and discussion

Au–Pd NPs/CFC electrodes were prepared from the aqueous solution of $HClO_4$, H_2SO_4 and $HAuCl_4/PdCl_2$ mixtures. So, we will name the metal nanoparticles prepared from the aqueous solutions of $HAuCl_4/PdCl_2$ mixtures in molar ratios of 5:1, 2:1, 1:1, 1:2 and 1:5 as Au_5Pd_1, Au_2Pd_1, Au_1Pd_1, Au_1Pd_2 and Au_1Pd_5 respectively.

To determine whether the bimetallic nanoparticles are aggregated metal particles or an alloy of the two metals, XRD analysis was performed. Fig. 1 shows the XRD patterns of the Au–Pd NPs/

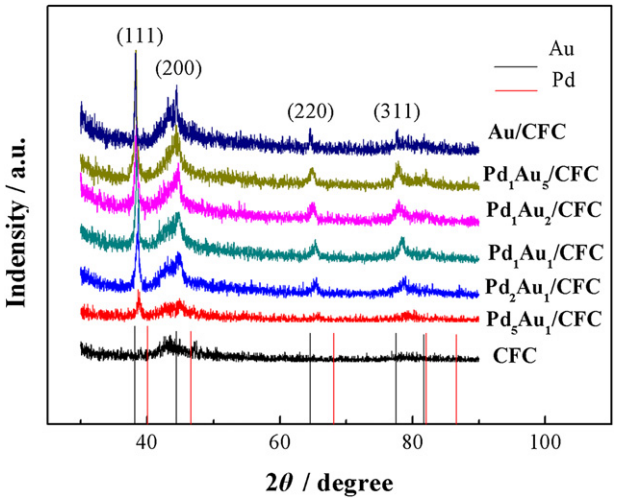

Fig. 1. XRD patterns of CFC and different materials prepared by potential pluse electrodeposition of Au and Pd from different concentrations of $HAuCl_4$ and $PdCl_2$.

CFC electrodes electrodeposited from different concentrations of $HAuCl_4$ and $PdCl_2$. There existed two broad peaks centered at about 43° and 80° in all samples, which can be associated with the carbon support. Each pattern of Au–Pd NPs/CFC exhibited four diffraction peaks in the range of $30° < 2\theta < 90°$ which can be indexed to diffraction from the (111), (200), (220) and (311) of the fcc structure of metallic Au and Pd. In addition, the diffraction peaks of the bimetallic particles showed a shift from their standard position of Au and Pd. This suggests that the prepared nanoparticles are Au–Pd alloys rather than a mixture of mono-metallic or core–shell nanoparticles.

Fig. 2 shows SEM images of CFC and the as-prepared Au–Pd NPs/CFC electrodes with different composition obtained by potential pulse electrodeposition. As seen on these images, all electrodeposited catalyst particles uniformly deposited on the carbon fibers. Also, it can be noted that the surface morphologies of the deposits depend on the composition of the electrolyte. The size of Au–Pd alloy nanoparticles increased as the Pd content increased. The diameters of Au–Pd NPs were in the range of 100–250 nm. It could be observed that Au–Pd NPs have the corrugated surface which provided a large surface area. Interestingly, it can be obviously found that the Au_1Pd_5 NPs showed a flower-like structure.

Different-magnification SEM images of Au_1Pd_5 NPs/CFC electrode in Fig. 3A and B reveal the flower-like Au–Pd nanoparticles which are uniformly deposited on the surface of carbon fibers. The surface of Au_1Pd_5 NPs consists of a lot nanoscale corrugations to form a flower-like structure which could remarkably increase the surface area, and the diameter of a single particle is around 200 nm. In order to get more insight into the structure of Au_1Pd_5 NPs, we also examined it by TEM and HRTEM. Fig. 3C is a TEM micrograph showing a single Au_1Pd_5 nanoparticle. The surface of the nanoparticle is not smooth, which is consistent with the SEM image. From the TEM image, a dark core surrounded by a light-color shell can be clearly distinguished. In accordance with the XRD analysis, it can be concluded that the flower-like Au_1Pd_5 NPs is Au–Pd alloy nanoparticles, indicating that the light-color shell is actually the thinner corrugations on the surface of nanoparticles. Furthermore, the corresponding energy dispersive X-ray (EDX) spectrum of Au_1Pd_5 NPs were analyzed to characterize the elemental composition of the particle in Fig. 3D. It can be observed that the spectrum of the EDX measurement shows the characteristic peaks of the metallic Au and Pd. The atomic ratio of Au and Pd is approximately 4:1 by EDX which is lower than that in the precursor. This is because the reduction potential of Au^{3+}/Au is much higher than that of Pd^{2+}/Pd. When applied to the pulse potential with the oxidation potential of 1.3 V and the reduction of 0 V, much more Au ions were reduced during the progress of electrodeposition. Fig. 4 shows the HRTEM image of a Au_1Pd_5 nanoparticle at different crystalline domains. In Fig. 4B–D, lines are drawn to highlight the different orientation of lattice fringes in each crystalline domain which suggests that the Au_1Pd_5 nanoparticle has the polycrystalline nature. Lattice planes of the crystal can be seen from this image.

The characterization of the surface of nanoparticles is a very important issue in the applications of nanoparticles such as catalysts and sensors. The surface of Au/CFC and Au–Pd NPs/CFC electrodes characterized electrochemically by CV in a 1.0 mol L^{-1} H_2SO_4 solution at a scan rate of 50 mV s^{-1} is shown in Fig. 5a. Typical redox responses corresponding to the oxidation and reduction of Au, Au–Pd alloy were observed at the nanoparticle-modified CFC electrodes. The observation of a single oxygen desorption peak with a potential value between those of Au and Pd for all the alloy nanoparticles demonstrates that the distribution of Au and Pd atoms on the surface of alloy nanoparticles is relatively homogeneous. Due to the small amount of Pd in Au–Pd nanoparticles which was shown in Table 1, the redox peaks of Au–Pd nanoparticles were in close proximity to Au. As the Pd content increased, the peaks gradually shifted negatively, also, the hydrogen adsorption/desorption peaks enhanced. Besides, the position of the reduction peak of Au and Au–Pd alloy electrodes varied in a linear manner with alloy composition and all Au–Pd/CFC electrodes had Au-enriched surfaces in Fig. 5b. Considering that the reduction potential of Au^{3+} is much higher than Pd^{2+}, it can be assumed that formation of the alloy particles should be initiated by nucleation of Au atoms followed by co-electrodeposition of residual Au and Pd atoms on the surface of the seeds at 0 V (the reduction potential of potential pluse electrodeposition) and then more Pd atoms are oxidizing to Pd^{2+} at 1.3 V (the oxidation potential of potential pluse electrodeposition) which make the higher Au content after manifold cycles. We have also demonstrated that the Pd^{2+} could not deposit on the CFC when applied the same electrochemical conditions. In addition, it can be found from Table 1 that the composition ratio of Au and Pd determined by EDX and ICP were not

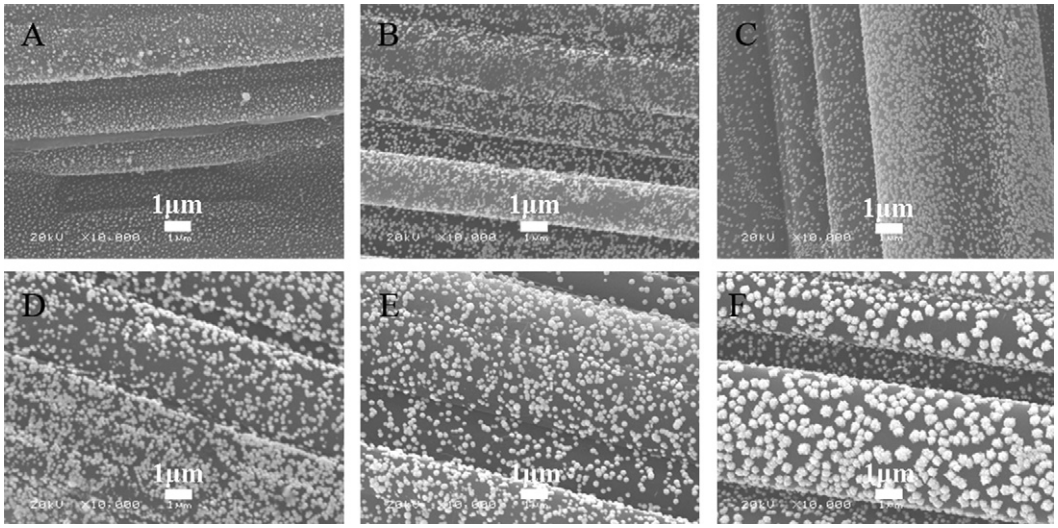

Fig. 2. SEM images of Au–Pd NPs/CFC electrodes with different concentrations of $HAuCl_4$ and $PdCl_2$. (A) Au NPs/CFC electrode; (B) Au_5Pd_1 NPs/CFC electrode; (C) Au_2Pd_1 NPs/CFC electrode; (D) Au_1Pd_1 NPs/CFC electrode; (E) Au_1Pd_2 NPs/CFC electrode; (F) Au_1Pd_5 NPs/CFC electrode.

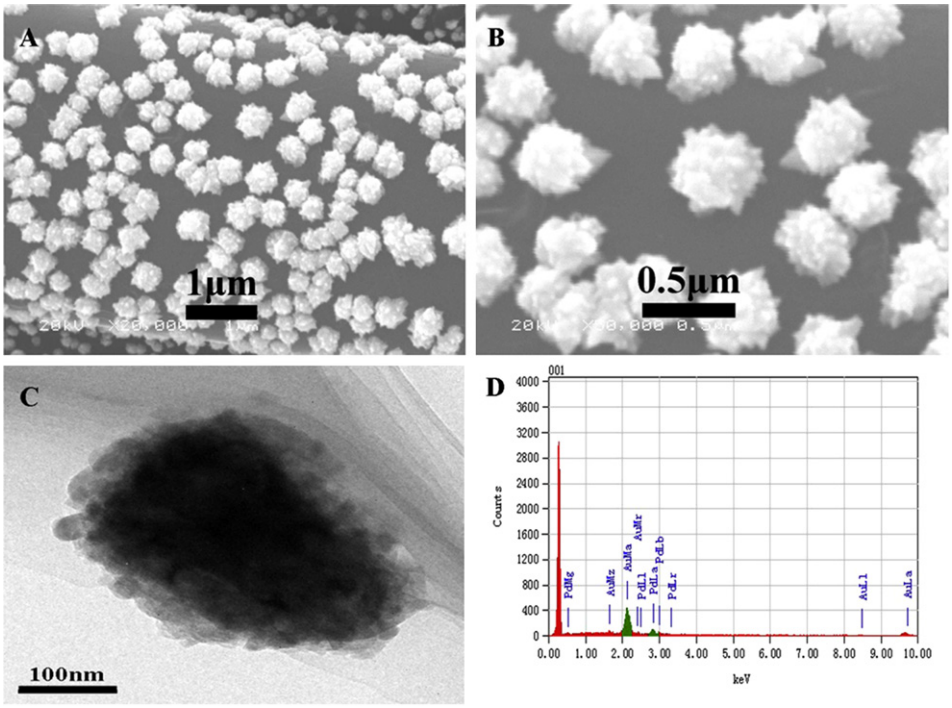

Fig. 3. (A) Low-magnification and (B) high-magnification SEM images of Au_1Pd_5 NPs/CFC electrode; (C) TEM image of Au_1Pd_5 NPs; (D) The corresponding EDX spectrum of Au_1Pd_5 NPs/CFC electrode.

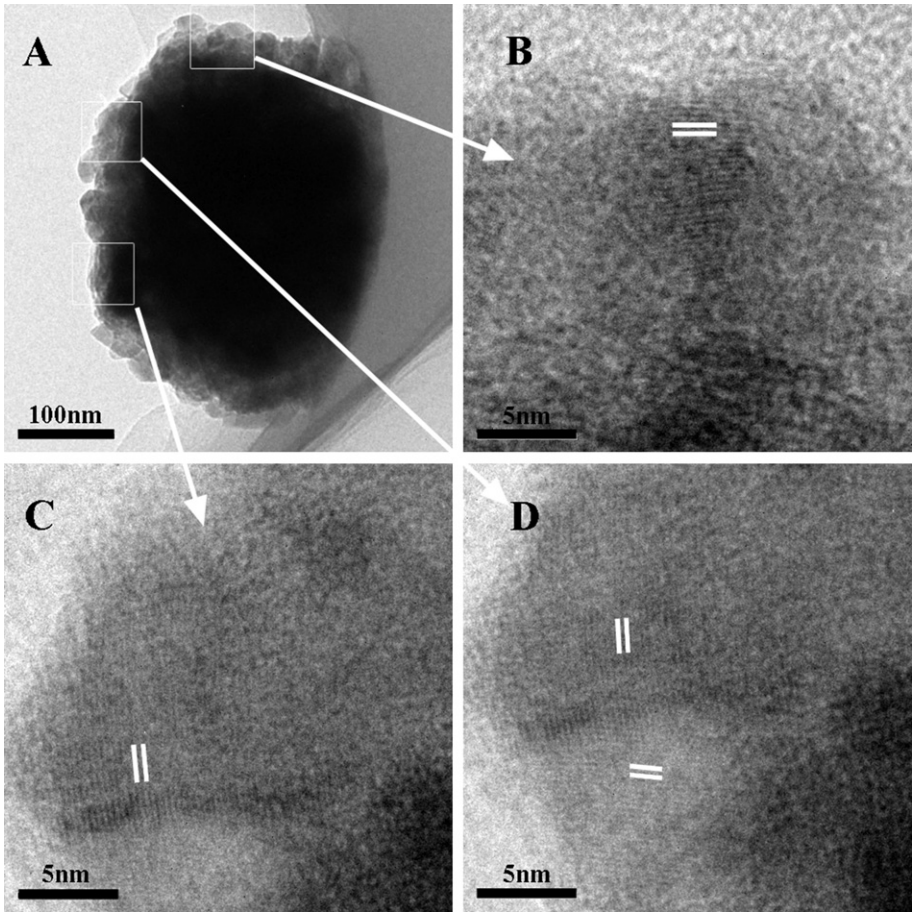

Fig. 4. (A) HRTEM image of a Au_1Pd_5 nanoparticle; (B–D) higher magnification images illustrate the nature of Au_1Pd_5 nanoparticle. White lines indicate the direction of lattice fringes in different crystalline domains.

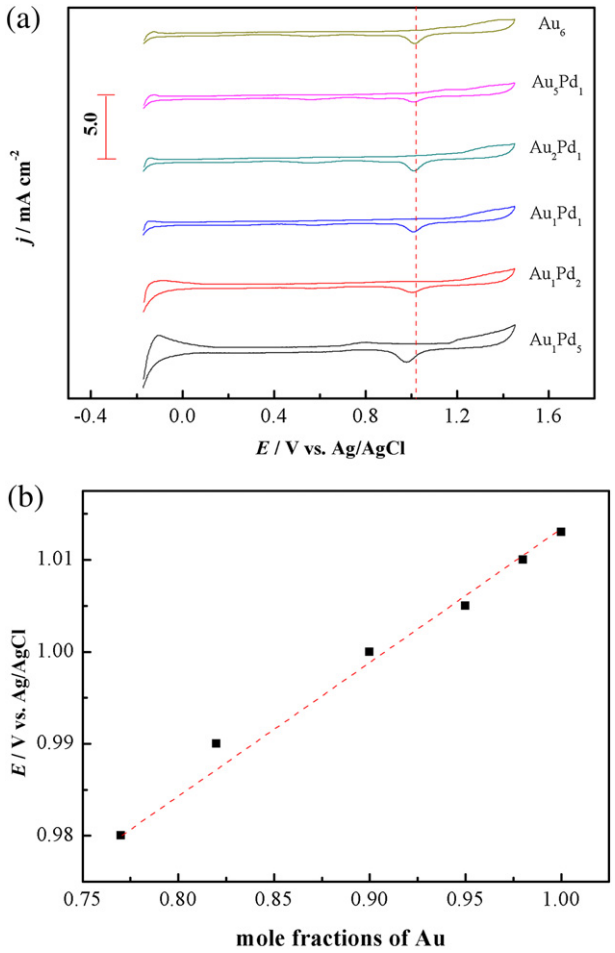

Fig. 5. (a) Cyclic voltammograms of Au–Pd NPs/CFC electrodes with different concentrations of $HAuCl_4$ and $PdCl_2$ in 1.0 mol L^{-1} H_2SO_4 solution at a scanning rate of 50 mV s^{-1}. (b) The position of the reduction peak of Au–Pd alloy nanoparticles supported on carbon fiber cloth.

consistent. In general, the EDX measurement examined the surface of metal distribution and ICP measurement tested the whole metal loading of nanoparticles. So it can be supposed that the Au and Pd atoms by co-electroreduction happen the rearrangement reaction which makes the rest of Pd atoms not to be oxidized.

The catalytic performance of Au/CFC and a series of Au–Pd NPs/CFC electrodes toward H_2O_2 electroreduction were investigated under acidic conditions. Fig. 6 shows the curves recorded in 1.0 mol L^{-1} H_2SO_4 + 0.5 mol L^{-1} H_2O_2 at a scanning rate of 10 mV s^{-1} with each catalysts supported on CFC. Indeed, the onset

Table 1
The composition and metal loading of different electrodeposited Au–Pd nanoparticles.

Sample name	The metal loading (mg cm^{-2})			Nanoparticle composition (Au–Pd) (%)	
	Au loading	Pd loading	Total	Determined by EDX	Determined by ICP
Au	0. 3038	0	0.3038	100-0	100-0
Au_5Pd_1	0.2466	0.0271	0.2737	98-2	90-10
Au_2Pd_1	0.2423	0.0406	0.2829	95-5	86-14
Au_1Pd_1	0.2106	0.0471	0.2577	90-10	82-18
Au_1Pd_2	0.1387	0.0435	0.1822	82-18	76-24
Au_1Pd_5	0.1073	0.0544	0.1617	77-23	67-33
Pd	0	0.0127	0.0127	0-100	0-100

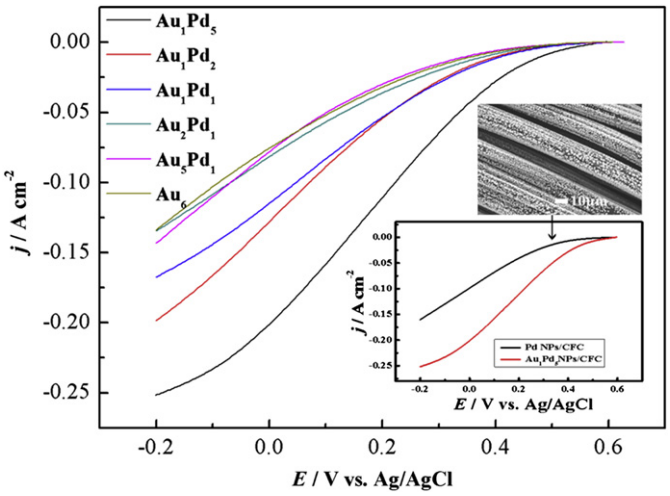

Fig. 6. The comparative polarization curves of Au–Pd NPs/CFC electrodes with different concentrations of $HAuCl_4$ and $PdCl_2$ in 1.0 mol L^{-1} H_2SO_4 + 0.5 mol L^{-1} H_2O_2 at a scanning rate of 10 mV s^{-1}. Insert is SEM image of Pd NPs/CFC electrode and the comparative polarization curves of Au_1Pd_5 NPs/CFC and Pd NPs/CFC.

potentials of H_2O_2 electroreduction became more positive with the increase of the Pd content. Also, the performance of Au–Pd NPs/CFC electrodes improved as the Pd content increased at the same potential which is owing to the higher activity of Pd than Au. It was also demonstrated that a small amount of incorporation of Pd can obviously improve the catalytic properties of Au. The current density could reach to 200 mA cm^{-2} at 0 V at the Au_1Pd_5 NPs/CFC electrode (Pd content is 23% in all by EDX). In order to compare the catalytic performance of the Au–Pd alloy nanoparticles with the pure Pd catalyst, CFC supported Pd particles (Pd NPs/CFC) were also prepared by potential pulse electrodeposition. The electrodeposition experiment was carried in the solution containing 5.0 mmol L^{-1} $PdCl_2$ and 0.1 mol L^{-1} $HClO_4$. The upper and lower potential were set at 0.65 V and 0.05 V, respectively, the deposition time was 20 min and the frequency was 100 Hz. As can be seen from the insert of Fig. 6, H_2O_2 reduction current density on the Au_1Pd_5 NPs/CFC electrode is much higher than that on the Pd NPs/CFC electrode (Pd loading is 0.2704 mg cm^{-2}). In addition, Au–Pd NPs/CFC electrode also exhibited better electrocatalytic activity than commercial Pd/C electrode for H_2O_2 electroreduction [38].

In order to further understand the electrochemical performance of H_2O_2 electroreduction at the Au–Pd NPs/CFC electrode in acid medium, we use the flower-like Au_1Pd_5 as an example, and the effects of H_2SO_4 concentration were systematically discussed in Fig. 7. The concentration of H_2O_2 was fixed at 0.5 mol L^{-1} and the concentration of H_2SO_4 varied from 1.0 to 4.0 mol L^{-1}. The onset potential was around 0.6 V, and the current densities increased with the potential going negatively. Notably, the curves of different H_2SO_4 concentrations were nearly the same before the potential of 0 V. It can be observed that the performance could not be improved as the concentration of H_2SO_4 increased. At −0.1 V, the current density reached to 232 mA cm^{-2} in the solution of 1.0 mol L^{-1} H_2SO_4 + 0.5 mol L^{-1} H_2O_2.

Fig. 8 shows the catalytic behavior of the Au_1Pd_5 NPs/CFC electrode in 2.0 mol L^{-1} H_2SO_4 solution containing H_2O_2 with various concentrations. The potential scans started from the open circuit potential and gone negatively. The electroreduction occurred at around 0.6 V independent of H_2O_2 concentration. The current densities increased with the increase of H_2O_2 concentration, yet the tendency became weaker at higher H_2O_2 concentration. We noticed that, when H_2O_2 concentration reaches 1.0 mol L^{-1}, the

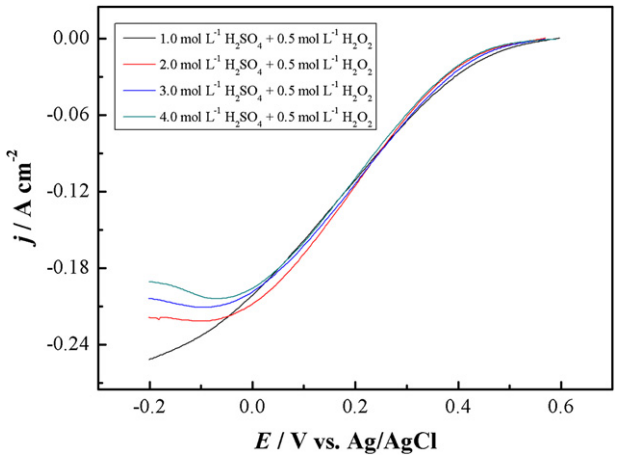

Fig. 7. Polarization curves for H_2O_2 electroreduction at the Au_1Pd_5 NPs/CFC electrode in x mol L^{-1} H_2SO_4 + 0.5 mol L^{-1} H_2O_2 (x = 1.0, 2.0, 3.0 and 4.0). Scan rate: 10 mV s^{-1}.

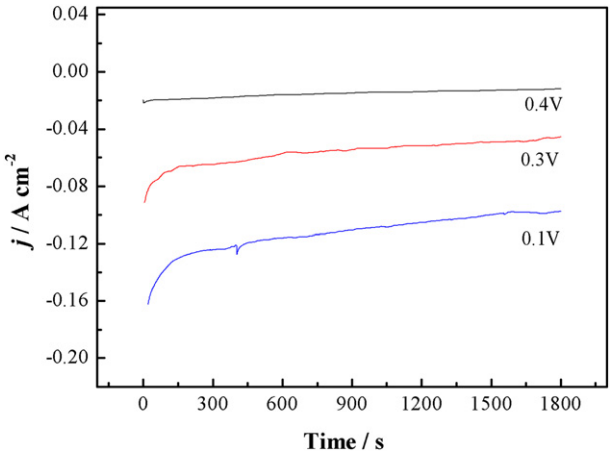

Fig. 9. Chronoamperometric curves for H_2O_2 electroreduction at different potentials in 2.0 mol L^{-1} H_2SO_4 + 0.5 mol L^{-1} H_2O_2.

decomposition of H_2O_2 becomes apparent and is more significant with the further increase of H_2O_2 concentration. Besides, the limiting current density was nonexistent with the H_2O_2 concentration higher than 0.5 mol L^{-1}, which implies that the reduction reaction was controlled by H_2O_2 diffusion.

The stability of Au_1Pd_5 NPs/CFC electrode for H_2O_2 electroreduction was investigated by chronoamperometric measurements. Fig. 9 shows chronoamperometric curves of H_2O_2 electroreduction in 2.0 mol L^{-1} H_2SO_4 + 0.5 mol L^{-1} H_2O_2 on the Au_1Pd_5 NPs/CFC electrode. The potentials were selected in the region according to the polarization curves in Fig. 8. At low potentials (0.4 V, the kinetics control region), the reduction currents reached steady-state quickly after constant potentials were applied and displayed no sign of decrease within the 30 min test period, At 0.3 V and 0.1 V (mixed control region), the current densities slightly decreased during the test which is because of the depletion of H_2O_2 near the electrode surface. In addition, the chronoamperometric curves for H_2O_2 electroreduction at three different potentials were tested using the same electrode, namely the electrode was tested for 5400 s, and the products from electroreduction of H_2O_2 could not lead to catalyst poisoning which is beneficial to keep active. The results in Fig. 9 indicate that the Au_1Pd_5 NPs/CFC electrode has a good stability for catalyzing H_2O_2 electroreduction.

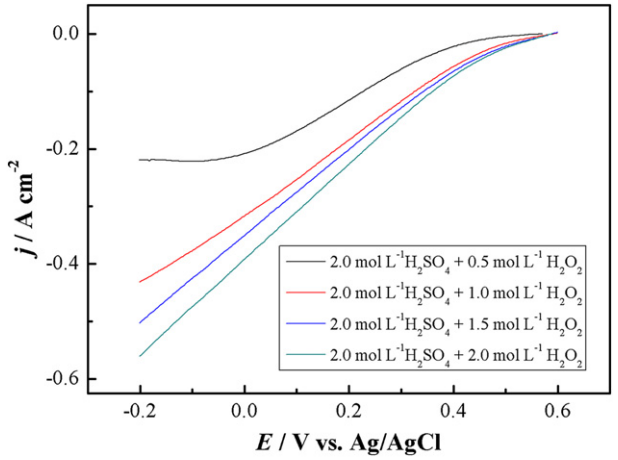

Fig. 8. Polarization curves for H_2O_2 electroreduction at the Au_1Pd_5 NPs/CFC electrode in 2.0 mol L^{-1} H_2SO_4 + x mol L^{-1} H_2O_2. (x = 0.5, 1.0, 1.5 and 2.0. Scan rate: 10 mV s^{-1}).

4. Conclusion

Au–Pd alloy nanoparticles supported on carbon fiber cloth (Au–Pd NPs/CFC) was successfully fabricated by potential pulse electrodeposition. The CFC is a promising substrate which could be also used as the current collector in a fuel cell. By changing the electrochemical conditions, different ratio of Au–Pd alloy nanoparticles are readily obtained. The catalytic performance toward H_2O_2 electroreduction in acid solution increased with the increase of Pd content. A small amount of incorporation of Pd can remarkably improve the catalytic properties of Au. Furthermore, it was also demonstrated that the flower-like Au–Pd NPs/CFC electrode displayed superior catalytic activity and good stability to H_2O_2 electroreduction.

Acknowledgments

We gratefully acknowledge the financial support of this research by Fundamental Research Funds for the Central Universities (HEUCFT1205), Harbin Science and Technology Innovation Fund for Excellent Academic Leaders (2012RFXXG103).

References

[1] J.H. Shim, J. Kim, C. Lee, Y. Lee, Chem. Mater. 23 (2011) 4694–4700.
[2] M. Li, Z. Wu, S.H. Overbury, J. Catal. 278 (2011) 133–142.
[3] W. Tang, A. He, Q. Liu, D.G. Ivey, Acta Mater. 56 (2008) 5818–5827.
[4] S. Jalili, A. Zeini Isfahani, R. Habibpour, Comput. Theor. Chem. 989 (2012) 18–26.
[5] Y.-H. Won, K. Huh, L.A. Stanciu, Biosens. Bioelectron. 26 (2011) 4514–4519.
[6] F. Cárdenas-Lizana, S. Gómez-Quero, C.J. Baddeley, M.A. Keane, Appl. Catal. A 387 (2010) 155–165.
[7] A. Sárkány, Z. Schay, K. Frey, É. Széles, I. Sajó, Appl. Catal. A 380 (2010) 133–141.
[8] G.C. Bond, Catal. Today 72 (2002) 5–9.
[9] Y. Song, Y. Ma, Y. Wang, J. Di, Y. Tu, Electrochim. Acta 55 (2010) 4909–4914.
[10] Y. Zhang, Y. Gu, S. Lin, J. Wei, Z. Wang, C. Wang, Y. Du, W. Ye, Electrochim. Acta 56 (2011) 8746–8751.
[11] H.M. Song, B.A. Moosa, N.M. Khashab, J. Mater. Chem. 22 (2012) 15953–15959.
[12] B. Pawelec, A.M. Venezia, V. La Parola, E. Cano-Serrano, J.M. Campos-Martin, J.L.G. Fierro, Appl. Surf. Sci. 242 (2005) 380–391.
[13] H. Matsumoto, K. Mitsuhara, A. Visikovskiy, T. Akita, N. Toshima, Y. Kido, Nucl. Instrum. Methods Phys. Res. Sect. B 268 (2010) 2281–2284.
[14] C. Ma, W. Ye, X. Shi, Y. Chang, Y. Chen, C. Wang, Appl. Surf. Sci. 255 (2009) 3713–3718.
[15] F. Liu, D. Wechsler, P. Zhang, Chem. Phys. Lett. 461 (2008) 254–259.
[16] A. Liang, Y. Zhang, Y. Fan, C. Chen, G. Wen, Q. Liu, C. Kang, Z. Jiang, Nanoscale 3 (2011) 3178–3184.
[17] W.C. Ketchie, M. Murayama, R.J. Davis, J. Catal. 250 (2007) 264–273.
[18] J.-W. Hu, Y. Zhang, J.-F. Li, Z. Liu, B. Ren, S.-G. Sun, Z.-Q. Tian, T. Lian, Chem. Phys. Lett. 408 (2005) 354–359.
[19] W. Hou, N.A. Dehm, R.W.J. Scott, J. Catal. 253 (2008) 22–27.

[20] H.C. Ham, G.S. Hwang, J. Han, S.W. Nam, T.H. Lim, J. Phys. Chem. C 114 (2010) 14922–14928.
[21] T. Garcia, R. Murillo, S. Agouram, A. Dejoz, M.J. Lazaro, L. Torrente-Murciano, B. Solsona, Chem. Commun. 48 (2012) 5316–5318.
[22] F. Gao, Y. Wang, D.W. Goodman, J. Phys. Chem. C 113 (2009) 14993–15000.
[23] J.K. Edwards, G.J. Hutchings, Angew. Chem. Int. Ed. 47 (2008) 9192–9198.
[24] J. Chai, F. Li, Y. Hu, Q. Zhang, D. Han, L. Niu, J. Mater. Chem. 21 (2011) 17922–17929.
[25] T. Balcha, J.R. Strobl, C. Fowler, P. Dash, R.W.J. Scott, ACS Catal. 1 (2011) 425–436.
[26] D.I. Enache, J.K. Edwards, P. Landon, B. Solsona-Espriu, A.F. Carley, A.A. Herzing, M. Watanabe, C.J. Kiely, D.W. Knight, G.J. Hutchings, Science 311 (2006) 362–365.
[27] M.-L. Wu, D.-H. Chen, T.-C. Huang, Langmuir 17 (2001) 3877–3883.
[28] R. Harpeness, A. Gedanken, Langmuir 20 (2004) 3431–3434.
[29] Y.W. Lee, M. Kim, Z.H. Kim, S.W. Han, J. Am. Chem. Soc. 131 (2009) 17036–17037.
[30] J. Xu, A.R. Wilson, A.R. Rathmell, J. Howe, M. Chi, B.J. Wiley, ACS Nano 5 (2011) 6119–6127.
[31] C. Shu, E. Wang, L. Jiang, Q. Tang, G. Sun, J. Power Sources 208 (2012) 159–164.
[32] D. Cao, Y. Gao, G. Wang, R. Miao, Y. Liu, Int. J. Hydrogen Energy 35 (2010) 807–813.
[33] D.M.F. Santos, P.G. Saturnino, R.F.M. Lobo, C.A.C. Sequeira, J. Power Sources 208 (2012) 131–137.
[34] O. Burheim, P.J.S. Vie, S. Møller-Holst, J. Pharoah, S. Kjelstrup, Electrochim. Acta 55 (2010) 935–942.
[35] H. Liu, L. Zhang, J. Zhang, D. Ghosh, J. Jung, B.W. Downing, E. Whittemore, J. Power Sources 161 (2006) 743–752.
[36] M. Carmo, M. Linardi, J.G. Rocha Poco, Int. J. Hydrogen Energy 33 (2008) 6289–6297.
[37] C. Ponce de León, F.C. Walsh, C.J. Patrissi, M.G. Medeiros, R.R. Bessette, R.W. Reeve, J.B. Lakeman, A. Rose, D. Browning, Electrochem. Commun. 10 (2008) 1610–1613.
[38] F. Yang, K. Cheng, Y. Mo, L. Yu, J. Yin, G. Wang, D. Cao, J. Power Sources 217 (2012) 562–568.